

# Dicke superposition probes for noise-resilient Heisenberg and super-Heisenberg Metrology

Sudha,<sup>1, 2,\*</sup> B. N. Karthik,<sup>1</sup> K. S. Akhilesh,<sup>3</sup> and A. R. Usha Devi<sup>4, 2</sup>

<sup>1</sup>*Department of Physics, Kuvempu University, Shankaraghatta-577 451, Karnataka, India*

<sup>2</sup>*Inspire Institute Inc., Alexandria, Virginia 22303, USA*

<sup>3</sup>*School of Computer Science and Engineering, RV University, Bangalore-560 059, Karnataka, India*

<sup>4</sup>*Department of Physics, Bangalore University, Bangalore-560 056, Karnataka, India*

(Dated: February 2, 2026)

Phase sensing with entangled multi-qubit states in the presence of noise is a central theme of modern quantum metrology. The present work investigates Dicke-state superposition probes for quantum phase sensing under parameter encoding generated by one- and two-body interaction Hamiltonians. A class of  $N$ -qubit Dicke superposition states that exhibit near-Heisenberg scaling  $F_Q \approx N^2$ , of the quantum Fisher information, while maintaining significantly enhanced robustness to dephasing noise compared to Greenberger–Horne–Zeilinger,  $W$ -superposition, and balanced Dicke states, under unitary encodings generated by one-body interaction Hamiltonians are identified. For two-body interactions, Dicke superposition probes optimizing the quantum Fisher information are identified, and their performance under phase-damping, amplitude-damping, and global depolarizing noise is explored. Within this family, certain Dicke superpositions are found to combine super-Heisenberg scaling with improved resilience to phase damping relative to Fisher-information-optimal probes. These results establish tailored near-optimal Dicke-state superposition probes as versatile and noise-resilient resources for Heisenberg and super-Heisenberg quantum phase sensing governed by one- and two-body interactions.

## I. INTRODUCTION

Quantum metrology exploits non-classical correlations to enhance the precision of parameter estimation beyond the standard quantum limit (SQL) [1–8]. Entangled multi-particle probe states and parameter-encoding Hamiltonian interactions play a key role in attaining quantum advantages in interferometry, spectroscopy and sensing platforms with atoms, photons and solid-state qubits [8–10]. A central question concerns the identification of multipartite entangled probes and parameter-encoding Hamiltonians that remain metrologically useful in noisy scenarios [6, 8, 10]. Recent literature has assessed quantum advantage in metrology by comparing the quantum Fisher information (QFI) of entangled probe states with separability bounds tailored to specific Hamiltonians, thereby identifying protocols that genuinely outperform all separable strategies [8–11]. In particular, Imai *et al.* [10] analyzed nonlinear Hamiltonians and derived general QFI-based criteria for metrologically useful entanglement beyond the case of non-interacting Hamiltonians, while Bhattacharyya *et al.* [11] investigated quantum sensing of even- versus odd-body interactions, demonstrating how nonlinear encoding Hamiltonians lead to distinct scaling behaviors and entanglement requirements [10, 11].

Most studies of noisy quantum phase sensing have focused on a restricted set of canonical probe families, such as Greenberger–Horne–Zeilinger (GHZ) states [3, 12, 13],  $W$  superpositions [14, 15], and Dicke states [16–18],

whose QFI scaling and noise robustness have been systematically studied. Beyond these standard probes, there is increasing interest in engineered superpositions of Dicke states [19–22]. From a foundational standpoint, such superpositions exhibit nontrivial multipartite quantum correlations — quantified, for example, by geometric measures of quantum discord [19] — that can persist even in regimes where entanglement is strongly suppressed by noise. From an experimental perspective, recent demonstrations of on-chip generation and coherent control of superpositions spanning the entire Dicke manifold [22] establish these states as readily accessible multipartite resources in state-of-the-art platforms. Together, these developments motivate a systematic investigation of the metrological role of tailored Dicke superpositions in noisy settings. In this paper, Dicke-state superposition probes are investigated for quantum phase sensing generated by one- and two-body qubit interaction Hamiltonians, with particular emphasis on scaling of QFI and robustness against dephasing, amplitude damping, and global depolarizing noise.

The organization of the paper is as follows. Section II reviews the basic framework of parameter estimation in quantum metrology. Tailored Dicke superposition states exhibiting near-Heisenberg scaling of the QFI for one-body interaction Hamiltonians are presented in Section III, and their noise robustness is compared with that of GHZ,  $W$ -superposition, and balanced Dicke probes. Section IV extends the analysis to two-body interaction Hamiltonians, identifying optimal and near-optimal Dicke superposition probes and examining their noise resilience. Section V gives a summary and concluding remarks.

\* tthdrs@gmail.com

## II. PARAMETER ESTIMATION AND FISHER INFORMATION

Parameter estimation is a core task underlying precision measurements in both classical and quantum metrology. Depending on the application, the parameter of interest may correspond to a frequency, phase, magnetic field, temperature, or other physical quantity to be estimated. Despite this diversity, any estimation protocol can be conceptually decomposed into three essential stages: (i) preparation of input probe, (ii) parameter encoding, and (iii) probe readout via optimal measurement and statistical inference.

### A. Classical Cramér-Rao bound

In classical parameter estimation, imperfections in probe preparation, system control, and measurement accuracy limit the achievable precision. For any unbiased estimator  $\hat{\theta}$  of a parameter  $\theta$  the ultimate precision  $\Delta\theta$  achievable in a classical parameter-estimation scheme is bounded from below by the Cramér-Rao bound [23, 24]

$$(\Delta\theta)^2 \geq \frac{1}{I(\theta)} \quad (1)$$

where

$$I(\theta) = \sum_x p(x|\theta) \left( \frac{\partial \ln p(x|\theta)}{\partial \theta} \right)^2 \quad (2)$$

is the classical Fisher information and  $p(x|\theta)$  denotes the probability of obtaining the outcome  $x$  for the random variable  $X$  used to estimate the parameter  $\theta$ . The Cramér-Rao bound sets the fundamental lower limit on the variance  $(\Delta\theta)^2$  of any unbiased estimator  $\hat{\theta}$  of a parameter  $\theta$  in classical estimation theory.

### B. Quantum parameter estimation

In the quantum scenario, the measurement precision is bounded by [23]

$$(\Delta\theta)^2 \geq \frac{1}{F_Q(\hat{\rho}, \hat{H})} \quad (3)$$

where  $F_Q(\hat{\rho}, \hat{H})$  denotes the QFI,  $\hat{\rho}$  corresponds to the probe state and  $\hat{H}$  is the Hamiltonian generating the unitary encoding  $\hat{U}(\theta) = e^{-i\hat{H}\theta}$ . After encoding, the probe state transforms to  $\hat{\rho}_\theta = \hat{U}(\theta) \hat{\rho} \hat{U}^\dagger(\theta)$ . Performing a generalized measurement described by a positive-operator-valued measure (POVM)  $\hat{E} \equiv \left\{ \hat{E}_x, \sum_x \hat{E}_x = I \right\}$  on the encoded state  $\hat{\rho}_\theta$  yields classical Fisher information

$$F(\theta) = \sum_x \frac{1}{p(x|\theta)} \left( \frac{\partial p(x|\theta)}{\partial \theta} \right)^2 \quad (4)$$

where

$$p(x|\theta) = \text{Tr}(\hat{E}_x \hat{\rho}_\theta).$$

The QFI  $F_Q(\hat{\rho}, \hat{H})$  is defined as the maximum of the classical Fisher information over all possible POVMs and sets the ultimate precision allowed by the quantum Cramér-Rao bound [1]:

$$F_Q(\hat{\rho}, \hat{H}) = \max_{\hat{\rho}, \hat{E}} F(\theta). \quad (5)$$

The QFI can, in principle, be attained by projective measurements in the eigenbasis of the symmetric logarithmic derivative (SLD) operator [1, 23]

$$\frac{\partial \hat{\rho}_\theta}{\partial \theta} = \frac{1}{2} (L(\hat{\rho}_\theta) \hat{\rho}_\theta + \hat{\rho}_\theta L(\hat{\rho}_\theta)) \quad (6)$$

in terms of which the QFI can be expressed as

$$F_Q(\hat{\rho}, \hat{H}) = \text{Tr}[\hat{\rho}_\theta L^2(\hat{\rho}_\theta)]. \quad (7)$$

The quantum Cramér-Rao bound (3) thus implies that, for a given metrological protocol specified by the probe state and the parameter-encoding Hamiltonian, the QFI  $F_Q(\hat{\rho}, \hat{H})$  quantifies the ultimate sensitivity of the probe state to minute changes in the parameter  $\theta$  being estimated.

For an arbitrary mixed probe state  $\hat{\rho} = \sum_i \lambda_i |\psi_i\rangle\langle\psi_i|$  under unitary encoding generated by a Hamiltonian  $\hat{H}$ , the QFI is given by [1]

$$F_Q(\hat{\rho}, \hat{H}) = 2 \sum_{i,j} \frac{(\lambda_i - \lambda_j)^2}{\lambda_i + \lambda_j} \left| \langle\psi_i|\hat{H}|\psi_j\rangle \right|^2, \quad (8)$$

where the sum runs over all indices satisfying  $\lambda_i + \lambda_j \neq 0$ . In the case of a pure probe state  $\hat{\rho} = |\psi\rangle\langle\psi|$ , the QFI reduces to

$$F_Q(|\psi\rangle, \hat{H}) = 4 \Delta^2 \hat{H} = 4 \left( \langle\psi|\hat{H}^2|\psi\rangle - \langle\psi|\hat{H}|\psi\rangle^2 \right), \quad (9)$$

where  $\Delta^2 \hat{H}$  denotes the variance of  $\hat{H}$  in the state  $|\psi\rangle$ .

For unitary parameter encoding on pure probe states, the maximal QFI achievable for a given Hamiltonian  $\hat{H}$  is given by

$$F_Q^{\max}(|\psi\rangle_{\text{opt}}, \hat{H}) = 4 \Delta^2 \hat{H} = (\lambda_{\max} - \lambda_{\min})^2, \quad (10)$$

where  $\lambda_{\max}$  and  $\lambda_{\min}$  denote the largest and smallest eigenvalues of  $\hat{H}$ , respectively. This bound is attained by the optimal probe state

$$|\psi\rangle_{\text{opt}} = \frac{|\phi_{\max}\rangle + |\phi_{\min}\rangle}{\sqrt{2}}, \quad (11)$$

where  $|\phi_{\max}\rangle$  and  $|\phi_{\min}\rangle$  are the eigenstates of the Hamiltonian  $\hat{H}$  corresponding to the eigenvalues  $\lambda_{\max}$  and  $\lambda_{\min}$  respectively. For any other choice of pure probe state, the

achievable QFI is given by Eq. (9), while for mixed probe states it is given by Eq. (8).

As an important example, consider the collective spin Hamiltonian

$$\hat{H} = \hat{\mathbf{J}} \cdot \hat{\mathbf{n}} \equiv \hat{\mathbf{J}}_n \quad (12)$$

where  $\hat{\mathbf{J}} = (\hat{J}_x, \hat{J}_y, \hat{J}_z)$  denotes the collective spin operator of an  $N$ -qubit system, with  $\hat{J}_\alpha = \frac{1}{2} \sum_i \hat{\sigma}_{i\alpha}$ ,  $\alpha = x, y, z$ ;  $\hat{\sigma}_{i\alpha}$  denoting the Pauli matrices of the  $i^{\text{th}}$  qubit, and  $\hat{\mathbf{n}}$  denotes a unit vector specifying the direction. The extremal eigenvalues of the Hamiltonian given by (12) are given by  $\lambda_{\max} = N/2$  and  $\lambda_{\min} = -N/2$ , yielding

$$F_Q = N^2 \quad (13)$$

and the optimal probe state achieving this bound is the  $N$ -qubit Greenberger–Horne–Zeilinger (GHZ) state [25],

$$|\text{GHZ}\rangle = \frac{1}{\sqrt{2}} (|0\rangle^{\otimes N} + |1\rangle^{\otimes N}). \quad (14)$$

In the following, quantum metrology protocols employing multiqubit probe states and single-parameter unitary encodings generated by one- and two-body interaction Hamiltonians will be discussed.

### C. Encoding with linear and nonlinear interactions

A wide range of metrological strategies for achieving high-precision measurements have been explored in the literature [8]. These approaches are commonly classified according to the nature of the Hamiltonian that encodes the parameter onto a  $N$ -qubit probe state. In linear (non-interacting or one-body interaction) quantum metrology [1, 6, 8, 23], the encoding multi-qubit Hamiltonian is given by Eq. (12). This Hamiltonian is linear in the probe constituent qubits and does not generate any entanglement during the encoding process. Collective, non-interacting generators of this form arise naturally in standard phase-estimation protocols and therefore provide a natural testbed for assessing the metrological utility of Dicke superposition probes.

In a parameter estimation protocol involving a linear parameter-encoding Hamiltonian and  $N$ -qubit separable probe states, the QFI scales as [8]

$$F_Q(\hat{\rho}_{\text{sep}}, \hat{H}) \propto N, \quad (15)$$

and correspondingly leads to the SQL or shot-noise limit (SNL) precision:

$$\Delta\theta \sim \frac{1}{\sqrt{N}}. \quad (16)$$

In contrast, genuinely entangled  $N$ -qubit probe states can achieve Heisenberg scaling [8, 26] of QFI under linear

Hamiltonian encoding, with  $F_Q(\hat{\rho}_{\text{ent}}, \hat{H}) \propto N^2$  in which case enhanced precision of estimation is achieved:

$$\Delta\theta \sim \frac{1}{N}. \quad (17)$$

In contrast, nonlinear metrology employs parameter-encoding Hamiltonians containing many-body interaction terms [10, 11, 27–56]. Typically, the collective spin Hamiltonians with  $k$ -body interactions of the form

$$\hat{H}_k = \left( \hat{\mathbf{J}}_n \right)^k = \sum_{i_1, \dots, i_k=1}^N \hat{\sigma}_n^{(i_1)} \dots \hat{\sigma}_n^{(i_k)}, \quad (18)$$

where the sum in (18) includes  $k$ -body interaction terms with  $i_1 < \dots < i_k$ ,  $k = 1, 2, \dots$  have been studied [10, 11]. For  $k > 1$ ,  $\hat{H}_k$  contains nonlinear  $k$ -body interactions generating the encoding unitary operation. Such encoding unitaries can dynamically generate quantum correlations, thereby allowing even initially separable probe states to surpass the SNL [27, 30, 35, 36]. It has been shown that the Hamiltonians containing  $k$ -body interaction terms can, in idealized settings, enable so-called super-Heisenberg precision scaling  $\Delta\theta \sim 1/N^k$  [28–30].

The metrological advantages predicted by both linear and nonlinear schemes are often severely degraded once realistic noise is taken into account [18, 21, 57–61]. A paradigmatic example is the  $N$ -qubit GHZ state, which attains Heisenberg-limited (HL) scaling for linear generators in the noiseless limit. However, GHZ states are extremely fragile to noise, and their metrological advantage diminishes quickly under decoherence. Analogous situations arise in nonlinear metrology: Although nonlinear Hamiltonians can, in principle, enable super-Heisenberg scaling in idealized metrological scenarios, realistic noise typically suppresses the achievable precision well below the ideal scaling of QFI. These limitations, imposed by inevitable noise, are not specific to any single class of probe states; rather, they reflect the general fragility of metrological advantages—linear or nonlinear—in realistic experimental conditions. Thus, a systematic evaluation of metrological performance under explicit noise models is crucial for identifying practically robust probes and sensing protocols. Accordingly, identifying probe states that combine high phase sensitivity with substantial noise resilience remains a key issue in quantum metrology.

The generators of the form (18) preserve permutation symmetry and therefore confine the unitary parameter-encoding strategy to the symmetric subspace. This motivates a detailed investigation on  $N$ -qubit permutation-symmetric Dicke superposition probes for noise-resilient quantum metrology with one- and two-body interaction Hamiltonians.

### III. DICKE SUPERPOSITION PROBES FOR NOISE-RESILIENT LINEAR METROLOGY

Multiqubit states that are invariant under interchange of qubits are extensively studied class of quantum states, notable both for their experimental relevance and their elegant mathematical structure [62–77]. Prominent examples include GHZ [25], W [78], and Dicke states [63]. States obeying symmetry under interchange of  $N$ -constituent qubits confine themselves to the  $(N+1)$ -dimensional subspace spanned by Dicke states

$$\begin{aligned} |D_{N-l,l}\rangle &\equiv \left|J = \frac{N}{2}, M = \frac{N}{2} - l\right\rangle, \quad l = 0, 1, \dots, N, \\ &= \sqrt{\frac{l!(N-l)!}{N!}} \sum_{\mathcal{P}} \mathcal{P} (|0\rangle^{\otimes N-l} \otimes |1\rangle^{\otimes l}), \quad (19) \end{aligned}$$

where  $\mathcal{P}$  runs over all distinct permutations of the qubits; this set  $\{|D_{N-l,l}\rangle\}$  of  $N+1$  basis states are simultaneous eigenstates of the collective spin operators  $\hat{J}^2 = \hat{J}_x^2 + \hat{J}_y^2 + \hat{J}_z^2$  and  $\hat{J}_z$ :

$$\begin{aligned} \hat{J}^2 |D_{N-l,l}\rangle &= \frac{N}{2} \left( \frac{N}{2} + 1 \right) |D_{N-l,l}\rangle \\ \hat{J}_z |D_{N-l,l}\rangle &= \left( \frac{N}{2} - l \right) |D_{N-l,l}\rangle. \quad (20) \end{aligned}$$

Recent experiments have demonstrated remarkable control over multiqubit Dicke states across diverse physical platforms, including photonic systems, cold atoms, and trapped ions [79–85]. Furthermore, state-of-the-art experiments have achieved on-chip generation and coherent collective control of superpositions spanning the full Dicke manifold [22], employing nanofabricated silicon photonic circuits with programmable interferometers to prepare up to eight-photon Dicke superpositions  $|D_{8-l,l}\rangle$  with  $l = 0, \dots, 8$ .

#### A. Linear metrology with Dicke superposition probes

For a Dicke-state probe  $|D_{N-l,l}\rangle$ , the QFI associated with unitary parameter encoding generated by the linear Hamiltonian  $\hat{H}_{k=1} = \hat{\mathbf{J}}_n$  (see Eq. (12)) is given by

$$\begin{aligned} F_Q(|D_{N-l,l}\rangle, \hat{H}_1) &= 4 \max_n (\Delta \hat{\mathbf{J}}_n)^2 \\ &= N + 2l(N-l), \quad l = 0, 1, 2, \dots, N. \quad (21) \end{aligned}$$

The optimal encoding direction lies in the  $XY$  plane. The QFI exhibits a quadratic dependence on the excitation number  $l$  and is maximized for  $l = N/2$  i.e.,  $F_Q(|D_{N-l,l}\rangle, \hat{H}_1) = N(N+2)/2$ . The resulting QFI scaling surpasses the SNL while remaining below the Heisenberg limit.

To assess whether this limitation can be overcome, superpositions of two distinct Dicke states (excluding GHZ

and W-superposition) are considered,

$$\begin{aligned} |D_{l,l'}^{(N)}\rangle &= \frac{1}{\sqrt{2}} (|D_{N-l,l}\rangle + |D_{N-l',l'}\rangle), \quad (22) \\ l &\neq l'; \quad l, l' = 1, 2, \dots, N-2; \quad N \geq 3. \end{aligned}$$

For Dicke superposition probes, the QFI  $F_Q(|D_{l,l'}^{(N)}\rangle, \hat{H}_1) = 4 \max_n (\Delta \hat{\mathbf{J}}_n)^2$  for choices of  $(l, l')$  yield a quadratic scaling with  $N$ . More specifically, the QFI for odd- $N$  superpositions with  $\frac{N}{2} - l = \mp \frac{1}{2}$ ,  $\frac{N}{2} - l' = \pm \frac{3}{2}$ , is evaluated to be

$$F_Q(|D_{l,l'}^{(N)}\rangle, \hat{H}_1) \approx 8.4641 + \frac{3}{4}(N-3)(N+5). \quad (23)$$

For even  $N$ , the optimal Dicke superpositions with  $\frac{N}{2} - l = \pm 1$ ,  $\frac{N}{2} - l' = \mp 1$ , the QFI is given by

$$F_Q(|D_{l,l'}^{(N)}\rangle, \hat{H}_1) = 4 + \frac{3}{4}(N-2)(N+4). \quad (24)$$

Representative values of the QFI for near-optimal Dicke superposition probes with  $N = 3-8$  are listed in Table I, illustrating  $\mathcal{O}(N^2)$  scaling.

TABLE I. QFI  $F_Q(|D_{l,l'}^{(N)}\rangle, \hat{H}_1) = 4 \max_n (\Delta \hat{\mathbf{J}}_n)^2$  for near-optimal Dicke-superposition probes  $|D_{l,l'}^{(N)}\rangle = (|D_{N-l,l}\rangle + |D_{N-l',l'}\rangle)/\sqrt{2}$  for  $N = 3-8$ . For each  $N$ , the listed pairs  $(l, l')$  maximize the QFI under linear collective-spin encoding generated by  $\hat{H}_1 = \hat{\mathbf{J}}_n$ . All cases exhibit  $\mathcal{O}(N^2)$  scaling.

$N$	$(l, l')$	$F_Q( D_{l,l'}^{(N)}\rangle, \hat{H}_1)$
3	$(\pm 2, 0)$	8.46
4	$(\pm 3, \mp 1)$	16
5	$(\pm 4, \mp 2)$	23.48
6	$(\pm 4, \mp 2)$	34
7	$(\pm 5, \mp 3)$	44.49
8	$(\pm 5, \mp 3)$	58

For the  $N$ -qubit W-superposition state  $|\bar{W}\bar{W}\rangle \equiv |D_{1,N-1}^{(N)}\rangle$ , corresponding to an equal superposition of the single-excitation Dicke state and its spin-flipped counterpart, the QFI under encoding by the optimal Hamiltonian  $\hat{H}_1 = \hat{J}_z$  is  $F_Q(|D_{1,N-1}^{(N)}\rangle, \hat{J}_z) = (N-2)^2$  for  $N \geq 6$ , which asymptotically approaches the Heisenberg-limit  $F_Q(|\text{GHZ}\rangle, \hat{J}_z) = N^2$  attained by the GHZ state [15].

Figure 1 compares the QFI of near-optimal Dicke superposition states  $|D_{l,l'}^{(N)}\rangle$  [Eqs. (23), (24)] with that of the W-superposition state  $|D_{1,N-1}^{(N)}\rangle$ , the balanced Dicke state [84, 86]  $|D_{N/2,N/2}\rangle$  (for even  $N$ ), and the GHZ state under collective spin encoding by  $\hat{J}_n$ . Over the range of system sizes shown, the Dicke superposition states considered here exhibit a systematic enhancement in QFI relative to the W-superposition state, with  $F_Q(|D_{l,l'}^{(N)}\rangle, \hat{J}_n) > F_Q(|D_{1,N-1}^{(N)}\rangle, \hat{J}_n)$  holding up to

$N \lesssim 20$ . This identifies an intermediate regime in which near-optimal Dicke superposition probes offer a systematic enhancement in QFI relative to the W-superposition states.

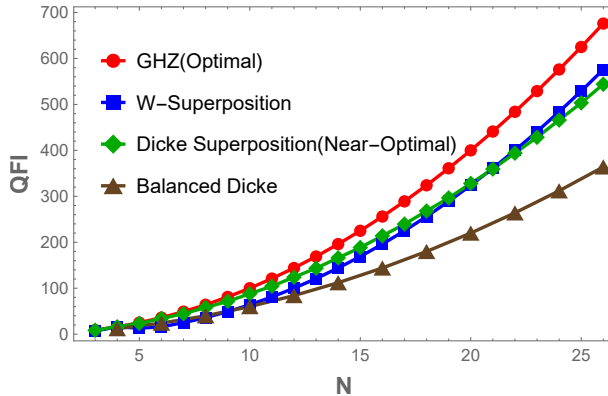


FIG. 1. QFI under collective spin encoding  $\hat{J}_n$  for near-optimal Dicke superposition states  $|D_{l,l'}^{(N)}\rangle$ , compared with the W-superposition state  $|D_{1,N-1}^{(N)}\rangle$ , the balanced Dicke state  $|D_{N/2,N/2}\rangle$  (for even  $N$ ), and the GHZ state. The Dicke superposition probes exhibit a modest but systematic enhancement in QFI relative to the W-superposition state over an intermediate regime  $N \lesssim 20$ .

## B. Noise resilience of near-optimal Dicke superposition states

The noise resilience of near-optimal Dicke superposition probes  $|D_{(N\pm 1)/2, (N\mp 3)/2}^{(\text{odd}N)}\rangle$ ,  $|D_{(N\pm 2)/2, (N\mp 2)/2}^{(\text{even}N)}\rangle$  under collective-spin encoding generated by  $\hat{J}_n$  is investigated below under three standard noise models: phase damping, amplitude damping, and global depolarization [87]. These noise models capture dominant decoherence mechanisms encountered in experimental platforms such as trapped ions [88], Rydberg-atom arrays [89], and cavity-mediated collective spin systems [90].

For local noise processes, the channel acts independently on each qubit, whereas global depolarization acts collectively on the full  $N$ -qubit state. A generic local noise channel is specified by single-qubit Kraus operators  $\{\hat{E}_k\}$  satisfying  $\sum_k \hat{E}_k^\dagger \hat{E}_k = \mathbb{I}_2$  and its action on an  $N$ -qubit state  $\hat{\rho}$  is given by

$$\hat{\rho}_{\text{noisy}} = \sum_{k_1, \dots, k_N} \left( \hat{E}_{k_1} \otimes \dots \otimes \hat{E}_{k_N} \right) \hat{\rho} \left( \hat{E}_{k_1}^\dagger \otimes \dots \otimes \hat{E}_{k_N}^\dagger \right). \quad (25)$$

The Kraus operators for amplitude damping are given by

$$\hat{E}_1 = |0\rangle\langle 0| + \sqrt{1-p}|1\rangle\langle 1|, \quad \hat{E}_2 = \sqrt{p}|0\rangle\langle 1|. \quad (26)$$

Phase damping is described by the Kraus operators

$$\begin{aligned} \hat{E}_1 &= \sqrt{1-p}\mathbb{I}_2, \quad \hat{E}_2 = \sqrt{p}|0\rangle\langle 0|, \\ \hat{E}_3 &= \sqrt{p}|1\rangle\langle 1| \end{aligned} \quad (27)$$

where  $\mathbb{I}_2$  denotes  $2 \times 2$  identity matrix. Global depolarization acts collectively and transforms the state as

$$\hat{\rho}_{\text{noisy}} = (1-p)\hat{\rho} + \frac{p}{2^N}\mathbb{I}_{2^N}, \quad (28)$$

For each noise model, the output state  $\hat{\rho}_{\text{noisy}}$  is evaluated from Eq. (25) or Eq. (28). The corresponding QFI is then computed using Eq. (8), and the phase sensitivity  $\Delta\theta$  is evaluated using the quantum Cramér–Rao bound, Eq. (3).

Figures 2 and 3 compare the noise robustness of the near-optimal Dicke superposition state with that of the corresponding W-superposition, GHZ, and balanced Dicke states for  $N = 8$ . Under phase damping, the Dicke superposition probe  $|D_{3,5}^{(8)}\rangle$  and the balanced Dicke state  $|D_{4,4}^{(8)}\rangle$  exhibit similar behavior, maintaining larger QFI over a broad range of noise strengths, outperform the GHZ and W-superposition probe  $|D_{1,7}^{(8)}\rangle$  (see Figs. 2(a), 3(a)). Under amplitude damping, the phase sensitivity of the balanced Dicke state lies between the SNL and the HL over a broader range of noise strengths than that of the GHZ, W-superposition, and near-optimal Dicke superposition states (see Fig. 3(b)). Under global depolarization, the optimal probe state (GHZ) and the near-optimal Dicke superposition state  $|D_{3,5}^{(8)}\rangle$  exhibit similar metrological behavior, maintaining phase sensitivity between the HL and SNL across almost the entire range of noise strengths (see Fig. 3(c)).

## IV. METROLOGY WITH COLLECTIVE TWO-BODY ENCODING HAMILTONIANS

Collective two-body interaction Hamiltonians constitute the simplest class of nonlinear generators in quantum metrology. Such interactions can generate metrologically useful entanglement during the encoding process itself, leading to enhanced scaling of the QFI and different classes of optimal probe states [8–11].

The present section focuses on representative two-body encoding Hamiltonians of the form  $\hat{J}_n^2$ . Non-linear interactions of this type underlie the Lipkin–Meshkov–Glick model [91], one-axis-twisting Hamiltonian [65]. The metrological performance of Dicke superposition probes under such two-body nonlinear encodings is analyzed here.

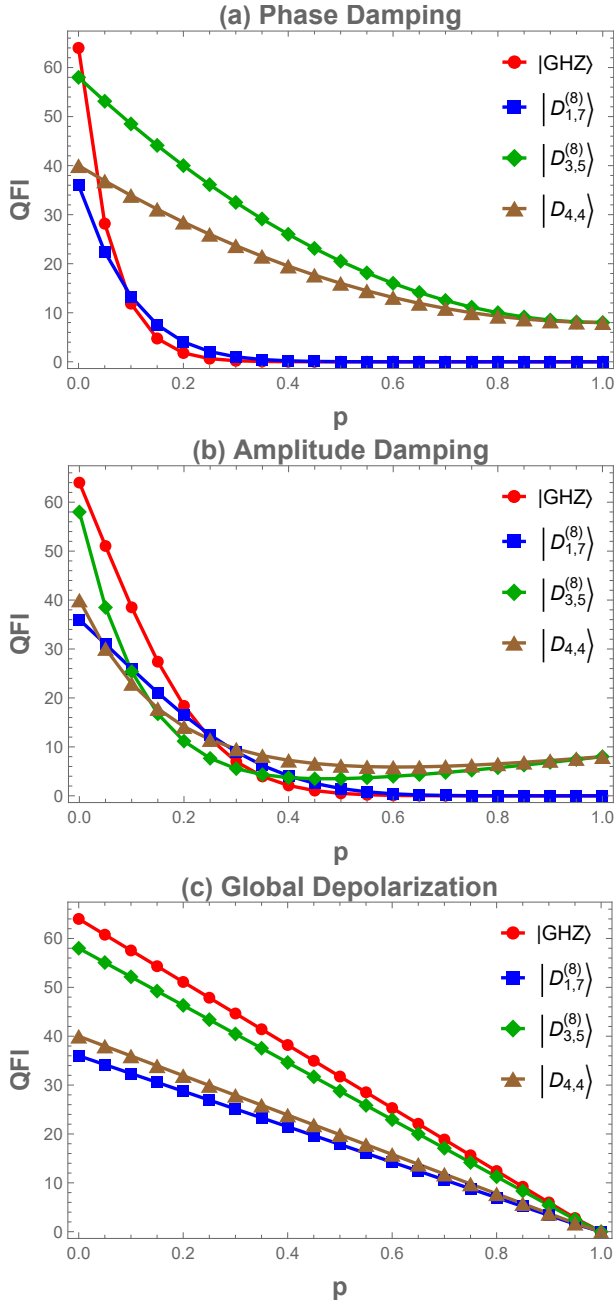


FIG. 2. QFI for  $N = 8$  probe states as a function of the noise parameter  $p$  under collective-spin encoding Hamiltonian  $\hat{H}_1 = \hat{J}_n$ . The near-optimal Dicke superposition state  $|D_{3,5}^{(8)}\rangle$  is compared with the GHZ, W-superposition state  $|D_{1,7}^{(8)}\rangle$ , and balanced Dicke state  $|D_{4,4}\rangle$  under (a) phase damping and (b) amplitude damping and (c) global depolarization.

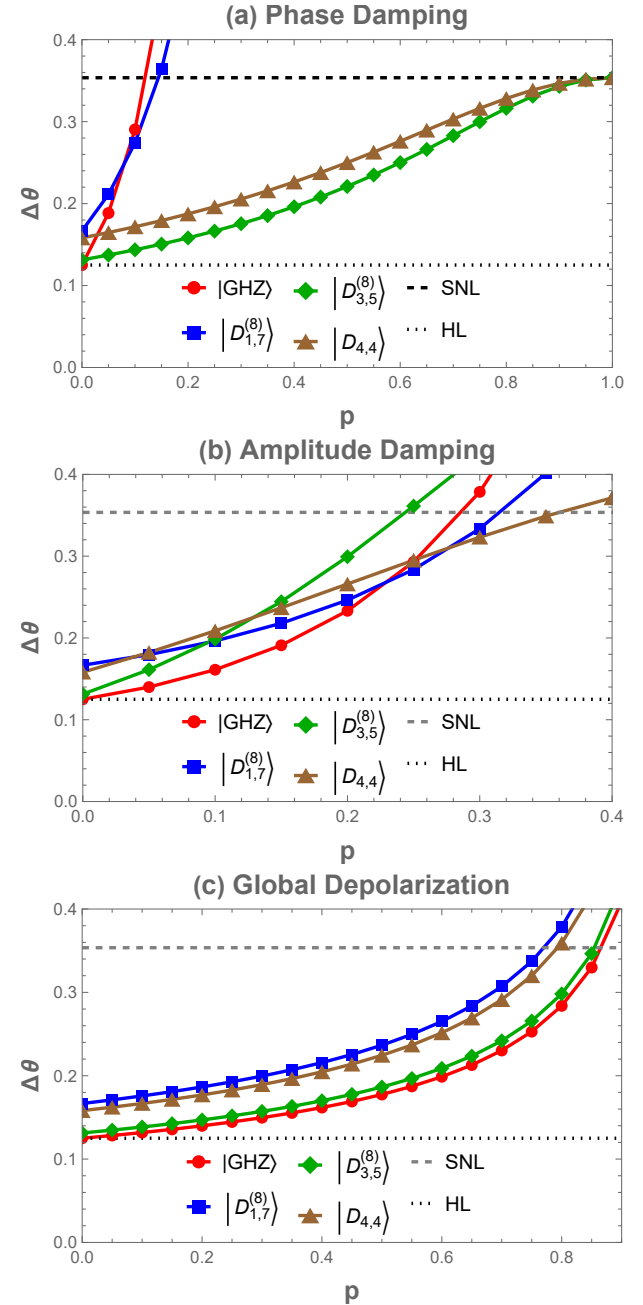


FIG. 3. Phase sensitivity  $\Delta\theta$  of  $N = 8$  probe states as a function of the noise parameter  $p$  under encoding Hamiltonian  $\hat{H}_1 = \hat{J}_n$ . The near-optimal Dicke superposition state  $|D_{3,5}^{(8)}\rangle$ , the GHZ state, the W-superposition state  $|D_{1,7}^{(8)}\rangle$ , and the balanced Dicke state  $|D_{4,4}\rangle$  are compared under (a) phase damping, (b) amplitude damping, and (c) global depolarization. The HL and the SNL are indicated for reference.

Consider the following encoding Hamiltonians:

$$\begin{aligned}
\hat{H}_2^{(1)} &= \eta \hat{J}_{\mathbf{n}}^2 = \frac{\eta}{4} \sum_{i,j=1}^N \hat{\sigma}_{i\mathbf{n}} \hat{\sigma}_{j\mathbf{n}} \\
\hat{H}_2^{(2)} &= \mu \hat{J}_{\mathbf{n}} + \eta \hat{J}_{\mathbf{n}}^2 \\
&= \frac{\mu}{2} \sum_{i=1}^N \hat{\sigma}_{i\mathbf{n}} + \frac{\eta}{4} \sum_{i,j=1}^N \hat{\sigma}_{i\mathbf{n}} \hat{\sigma}_{j\mathbf{n}} \\
\hat{H}_2^{(3)} &= \frac{\eta}{4} \sum_{i < j}^N \hat{\sigma}_{i\mathbf{n}} \hat{\sigma}_{j\mathbf{n}} = \frac{\eta}{2} \left( \hat{J}_{\mathbf{n}}^2 - \frac{N}{4} \mathbb{I}_{2^N} \right), \\
\hat{H}_2^{(4)} &= \frac{\mu}{2} \sum_{i=1}^N \hat{\sigma}_{i\mathbf{n}} + \frac{\eta}{4} \sum_{i < j}^N \hat{\sigma}_{i\mathbf{n}} \hat{\sigma}_{j\mathbf{n}} \\
&= \mu \hat{J}_{\mathbf{n}} + \frac{\eta}{2} \left( \hat{J}_{\mathbf{n}}^2 - \frac{N}{4} \mathbb{I}_{2^N} \right), \tag{29}
\end{aligned}$$

where  $\mu$  and  $\eta$  denote the strengths of the linear and two-body nonlinear interactions, respectively. Throughout this work, we set  $\mu = 1 = \eta$  for simplicity of analysis.

The QFI corresponding to pure optimal input probe states  $|\psi^{(r)}\rangle_{\text{opt}}$  and encoding Hamiltonians  $\hat{H}_2^{(r)}$ ,  $r = 1, 2, 3, 4$  (see Eq. (29)) is given by (see Eq.(10))  $F_Q(|\psi^{(r)}\rangle_{\text{opt}}, \hat{H}_2^{(r)}) = 4\Delta^2 \hat{H}_2^{(r)} = (\lambda_{\max}^{(r)} - \lambda_{\min}^{(r)})^2$ , where  $\lambda_{\max}^{(r)}$  and  $\lambda_{\min}^{(r)}$  are the respective maximum and minimum eigenvalues of the encoding Hamiltonian  $\hat{H}_2^{(r)}$ . The optimal probe state is  $|\psi^{(r)}\rangle_{\text{opt}} = (|\phi_{\max}^{(r)}\rangle + |\phi_{\min}^{(r)}\rangle)/\sqrt{2}$  with  $|\phi_{\max}^{(r)}\rangle, |\phi_{\min}^{(r)}\rangle$  denoting the eigenstates corresponding respectively to the eigenvalues  $\lambda_{\max}^{(r)}, \lambda_{\min}^{(r)}$  of  $\hat{H}_2^{(r)}$ ,  $r = 1, 2, 3, 4$ .

Note that the eigenstates of the collective spin operator  $\hat{J}_{\mathbf{n}}$  and its square  $\hat{J}_{\mathbf{n}}^2$  are the Dicke states  $|D_{N-l,l}\rangle_{\mathbf{n}}$ ,  $l = 0, 1, \dots, N$  with respect to the quantization axis  $\hat{\mathbf{n}}$  and the associated eigenvalues given by  $(N/2)-l, ((N/2)-l)^2$  respectively. The maximum eigenvalue of  $\hat{J}_{\mathbf{n}}$  is  $N/2$ , while that of  $\hat{J}_{\mathbf{n}}^2$  is  $N^2/4$ . The latter is two-fold degenerate, with the corresponding eigenstates  $|D_{N,0}\rangle_{\mathbf{n}} = |0\rangle_{\mathbf{n}}^{\otimes N}$ , and  $|D_{0,N}\rangle_{\mathbf{n}} = |1\rangle_{\mathbf{n}}^{\otimes N}$ . For the two-body encoding Hamiltonian  $\hat{H}_2^{(1)} = \hat{J}_{\mathbf{n}}^2$ , an equal-weight superposition of these two extremal eigenstates  $|\text{GHZ}\rangle_{\mathbf{n}} = (|0\rangle_{\mathbf{n}}^{\otimes N} + |1\rangle_{\mathbf{n}}^{\otimes N})/\sqrt{2}$  is therefore an eigenstate associated with the maximum eigenvalue  $N^2/4$ .

The minimum eigenvalue of  $\hat{J}_{\mathbf{n}}$  is  $-N/2$ , with the corresponding eigenstate  $|D_{0,N}\rangle_{\mathbf{n}} = |1\rangle_{\mathbf{n}}^{\otimes N}$ . In contrast, the minimum eigenvalue of  $\hat{J}_{\mathbf{n}}^2$  depends on the parity of  $N$ . For odd  $N$ , the minimum eigenvalue is  $1/4$ , with the corresponding eigenstate  $|D_{(N-1)/2,(N+1)/2}\rangle_{\mathbf{n}}$ . For even  $N$ , minimum eigenvalue is zero, with the corresponding eigenstate equal to  $|D_{N/2,N/2}\rangle_{\mathbf{n}}$ .

The eigenvalues  $\lambda_{\max}^{(r)}, \lambda_{\min}^{(r)}$ , the corresponding eigenvectors  $|\phi_{\max}^{(r)}\rangle, |\phi_{\min}^{(r)}\rangle$  of  $\hat{H}_2^{(r)}$ ,  $r = 1, 2, 3, 4$  along with the QFI  $F_Q(|\psi^{(r)}\rangle_{\text{opt}}, \hat{H}_2^{(r)})$  are summarized in Table II

The optimal probe states  $|\psi^{(r)}\rangle_{\text{opt}}$  maximizing

the QFI for the two-body encoding Hamiltonians  $\hat{H}_2^{(r)}$ ,  $r = 1, 2, 3, 4$  (see Eq. (29)) are given by

$$\begin{aligned}
|\psi_{N=\text{odd}}^{(1)}\rangle &= \frac{1}{\sqrt{2}} \left( |\text{GHZ}\rangle_{\mathbf{n}} + |D_{(N-1)/2,(N+1)/2}\rangle_{\mathbf{n}} \right) \\
|\psi_{N=\text{even}}^{(1)}\rangle &= \frac{1}{\sqrt{2}} \left( |\text{GHZ}\rangle_{\mathbf{n}} + |D_{N/2,N/2}\rangle_{\mathbf{n}} \right) \\
|\psi_{N=\text{odd}}^{(2)}\rangle &= \frac{1}{\sqrt{2}} \left( |0\rangle_{\mathbf{n}}^{\otimes N} + |D_{(N-1)/2,(N+1)/2}\rangle_{\mathbf{n}} \right) \\
|\psi_{N=\text{even}}^{(2)}\rangle &= \frac{1}{\sqrt{2}} \left( |0\rangle_{\mathbf{n}}^{\otimes N} + |D_{N/2,(N+2)/2}\rangle_{\mathbf{n}} \right) \tag{30} \\
|\psi_{N=\text{odd}}^{(3)}\rangle &= |\psi_{N=\text{odd}}^{(1)}\rangle \\
|\psi_{N=\text{even}}^{(3)}\rangle &= |\psi_{N=\text{even}}^{(1)}\rangle \\
|\psi_{N=\text{odd}}^{(4)}\rangle &= \frac{1}{\sqrt{2}} \left( |0\rangle_{\mathbf{n}}^{\otimes N} + |D_{(N+1)/2,(N+3)/2}\rangle_{\mathbf{n}} \right) \\
|\psi_{N=\text{even}}^{(4)}\rangle &= \frac{1}{\sqrt{2}} \left( |0\rangle_{\mathbf{n}}^{\otimes N} + |D_{(N-2)/2,(N+2)/2}\rangle_{\mathbf{n}} \right)
\end{aligned}$$

For metrological schemes based on nonlinear  $k$ -body generators, the precision benchmarks differ markedly from those of linear encodings [28–30]. While optimal separable probes yield [10] a Fisher information scaling  $\mathcal{O}(N^{2k-1})$ , entangled states can achieve the scaling [10, 11, 28–30]  $\mathcal{O}(N^{2k})$ , corresponding to a separable state precision bound  $\Delta\theta \sim N^{-(k-\frac{1}{2})}$  and the nonlinear Heisenberg limit  $\Delta\theta \sim N^{-k}$ .

These two regimes are denoted here as the nonlinear shot-noise limit (NL-SNL) and the nonlinear Heisenberg limit (NL-HL), respectively. A probe state whose phase sensitivity satisfies

$$(\Delta\theta)_{\text{NL-HL}} \leq \Delta\theta < (\Delta\theta)_{\text{NL-SNL}} \tag{31}$$

exhibits a genuine metrological advantage over separable probes and constitutes a practically useful quantum resource.

Table III summarizes the nonlinear metrological performance of the two-body interaction Hamiltonians  $\hat{H}_2^{(r)}$ ,  $r = 1, 2, 3, 4$  for  $N = 8$ . Here, the second column displays the maximum Fisher information  $F_Q(|\psi\rangle_{\text{sep}}, \hat{H}_2^{(r)})$  for separable probe states, which sets the nonlinear shot-noise reference. The third column lists the Fisher information  $F_Q(|\psi_{(2)}^{(N=8)}\rangle_{\mathbf{n}}, \hat{H}_2^{(r)})$  for the optimal probe state. The last two columns translate these Fisher informations into corresponding phase sensitivities  $(\Delta\theta)_{\text{NL-SNL}}$  and  $(\Delta\theta)_{\text{NL-HL}}$ , respectively.

### A. Near-optimal Dicke superposition probes for nonlinear two-body encodings

Dicke superposition states  $|D_{l,l'}^{(N)}\rangle$  were introduced in Sec. II in the context of linear (non-interacting) metrology, where they were shown to provide near-optimal phase sensitivity. It is natural to explore whether the

TABLE II. Eigenvalues  $\lambda_{\max}^{(r)}$ ,  $\lambda_{\min}^{(r)}$ , corresponding eigenstates  $|\phi_{\max}^{(r)}\rangle$ ,  $|\phi_{\min}^{(r)}\rangle$  of the two-body encoding Hamiltonians  $\hat{H}_2^{(r)}$  ( $r = 1, 2, 3, 4$ ), along with the resulting quantum Fisher information  $F_Q(|\psi^{(r)}\rangle_{\text{opt}}, \hat{H}_2^{(r)})$ . Throughout the table, Dicke states  $|D_{N-l,l}\rangle_{\mathbf{n}}$ , Dicke superposition states  $|D_{l,l'}^{(N)}\rangle_{\mathbf{n}}$ , and computational basis states  $|0\rangle_{\mathbf{n}}$ ,  $|1\rangle_{\mathbf{n}}$  are all defined with respect to the quantization axis  $\hat{\mathbf{n}}$ .

	$\hat{H}_2^{(1)} = \hat{J}_{\mathbf{n}}^2$	$\hat{H}_2^{(2)} = \hat{J}_{\mathbf{n}} + \hat{J}_{\mathbf{n}}^2$	$\hat{H}_2^{(3)} = \frac{1}{2} \left( \hat{J}_{\mathbf{n}}^2 - \frac{N}{4} \mathbb{I}_{2^N} \right)$	$\hat{H}_2^{(4)} = \hat{J}_{\mathbf{n}} + \frac{1}{2} \left( \hat{J}_{\mathbf{n}}^2 - \frac{N}{4} \mathbb{I}_{2^N} \right)$
$\lambda_{\max}^{(r)}$	$N^2/4$	$N(N+2)/4$	$N(N-1)/8$	$N(N+3)/8$
$\lambda_{\min}^{(r)}$ (odd $N$ )	$1/4$	$-1/4$	$-N/8$	$-(N+3)/8$
$\lambda_{\min}^{(r)}$ (even $N$ )	$0$	$0$	$-N/8$	$-(N+4)/8$
$ \phi_{\max}^{(r)}\rangle$	$ \text{GHZ}\rangle_{\mathbf{n}}$	$ 0\rangle_{\mathbf{n}}^{\otimes N}$	$ \text{GHZ}\rangle_{\mathbf{n}}$	$ 0\rangle_{\mathbf{n}}^{\otimes N}$
$ \phi_{\min}^{(r)}\rangle$ (odd $N$ )	$ D_{(N-1)/2,(N+1)/2}^{(N)}\rangle_{\mathbf{n}}$	$ D_{(N-1)/2,(N+1)/2}^{(N)}\rangle_{\mathbf{n}}$	$ D_{(N-1)/2,(N+1)/2}^{(N)}\rangle_{\mathbf{n}}$	$ D_{(N+1)/2,(N+3)/2}^{(N)}\rangle_{\mathbf{n}}$
$ \phi_{\min}^{(r)}\rangle$ (even $N$ )	$ D_{N/2,N/2}\rangle_{\mathbf{n}}$	$ D_{N/2,(N+2)/2}^{(N)}\rangle_{\mathbf{n}}$	$ D_{N/2,N/2}\rangle_{\mathbf{n}}$	$ D_{(N-2)/2,(N+2)/2}\rangle_{\mathbf{n}}$
$F_Q$ (odd $N$ )	$(N^2 - 1)^2/16$	$(N+1)^4/16$	$(N^2 - 1)^2/64$	$(N+3)^2(N+1)^2/64$
$F_Q$ (even $N$ )	$N^4/16$	$N^2(N+2)^2/16$	$N^4/64$	$(N+2)^4/64$

TABLE III. Nonlinear metrological benchmarks for two-body Hamiltonians  $\hat{H}_2^{(r)}$ ,  $r = 1, 2, 3, 4$  (See Eqs. (29)) for  $N = 8$ . The QFI  $F_Q(|\psi\rangle_{\text{sep}}, \hat{H}_2^{(r)})$  achievable by separable states, the QFI  $F_Q(|\psi_{(N=8)}^{(r)}\rangle_{\mathbf{n}}, \hat{H}_2^{(r)})$  for the near-optimal Dicke superposition probe  $|\psi_{(N=8)}^{(r)}\rangle_{\mathbf{n}}$ , and the corresponding phase sensitivities  $(\Delta\theta)_{\text{NL-SNL}}$ ,  $(\Delta\theta)_{\text{NL-HL}}$  are listed in columns 2 - 5.

$\hat{H}_2^{(r)}$	$F_Q( \psi\rangle_{\text{sep}}, \hat{H}_2^{(r)})$	$F_Q( \psi_{(N=8)}^{(r)}\rangle_{\mathbf{n}}, \hat{H}_2^{(r)})$	$(\Delta\theta)_{\text{NL-SNL}}$	$(\Delta\theta)_{\text{NL-HL}}$
$\hat{H}_2^{(1)}$	105.54	256	0.097	0.063
$\hat{H}_2^{(2)}$	151.65	400	0.081	0.05
$\hat{H}_2^{(3)}$	26.39	64	0.195	0.125
$\hat{H}_2^{(4)}$	52.14	144	0.138	0.083

same class of probes retains its metrological usefulness in the presence of nonlinear, two-body encoding Hamiltonians.

In the present context, the encoding dynamics is generated by collective two-body Hamiltonians  $\hat{H}_2^{(r)}$ ,  $r = 1, 2, 3, 4$  (see Eqs.(29)). The Fisher information is evaluated for Dicke superposition probes and optimized over the indices  $(l, l')$  for fixed system size. The resulting near-optimal Dicke superposition states and their corresponding Fisher information values for  $N = 5-8$  are summarized in Table IV. Noise robustness of the optimal probe states and the near-optimal Dicke superposition

states (encoded by the non-linear two-body interaction Hamiltonians  $\hat{H}_2^{(r)}$ ,  $r = 1, 2, 3, 4$ ) is investigated in the following subsection.

### B. Noise resilience of optimal and near-optimal Dicke superposition probes in two-body metrology

The noise robustness of the optimal and near-optimal Dicke superposition probe states via two-body interaction Hamiltonians is now analyzed under realistic decoherence mechanisms. In particular, metrological performance of these probes under local phase damping, local amplitude damping, and global depolarizing noise is studied. The impact of these three noise processes on the Fisher information of the identified probe states is summarized in Figures 4–7. Figure 4 displays the phase sensitivity of the optimal probe state  $|\psi_{(N=8)}^{(2)}\rangle_{\mathbf{n}} = \frac{1}{\sqrt{2}} (|0\rangle_{\mathbf{n}}^{\otimes 8} + |D_{4,5}^{(8)}\rangle_{\mathbf{n}})$  for  $N = 8$ , subjected to three different noises after encoding the state using the Hamiltonian  $\hat{H}_2^{(2)} = \hat{J}_{\mathbf{n}} + \hat{J}_{\mathbf{n}}^2$ . It is observed, in general, that the optimal probes are particularly susceptible to local phase damping while exhibiting comparatively better resilience against amplitude damping and global depolarization, when they are encoded using two-body interaction Hamiltonians given in Eqs.(29). Figures 5–7 present a direct comparison between the optimal probe states (see Eqs. (30)) and the near-optimal Dicke superposition

TABLE IV. The QFI of near-optimal Dicke superposition probe states  $|D_{l,l'}^{(N)}\rangle_n \equiv (|D_{N-l,l}\rangle_n + |D_{N-l',l'}\rangle_n)/\sqrt{2}$  for  $N = 5 - 8$  with respect to quantization axis  $\hat{\mathbf{n}}$  for collective two-body encoding Hamiltonians  $\hat{H}_2^{(r)}$  ( $r = 1, 2, 3, 4$ ).

	$\hat{H}_2^{(1)} = \hat{J}_{\mathbf{n}}^2$	$\hat{H}_2^{(2)} = \hat{J}_{\mathbf{n}} + \hat{J}_{\mathbf{n}}^2$	$\hat{H}_2^{(3)} = \frac{1}{2} \left( \hat{J}_{\mathbf{n}}^2 - \frac{N}{4} \mathbb{I}_{2^N} \right)$	$\hat{H}_2^{(4)} = \hat{J}_{\mathbf{n}} + \frac{1}{2} \left( \hat{J}_{\mathbf{n}}^2 - \frac{N}{4} \mathbb{I}_{2^N} \right)$
$N = 5$	$F_Q( D_{0,4}^{(5)}\rangle_n, \hat{H}_2^{(1)}) \simeq 33.67$	$F_Q( D_{0,2}^{(5)}\rangle_n, \hat{H}_2^{(2)}) \simeq 72.37$	$F_Q( D_{0,4}^{(5)}\rangle_n, \hat{H}_2^{(3)}) \simeq 8.41$	$F_Q( D_{0,2}^{(5)}\rangle_n, \hat{H}_2^{(4)}) \simeq 33.9$
$N = 6$	$F_Q( D_{1,5}^{(6)}\rangle_n, \hat{H}_2^{(1)}) \simeq 79.75$	$F_Q( D_{0,2}^{(6)}\rangle_n, \hat{H}_2^{(2)}) \simeq 134.47$	$F_Q( D_{1,5}^{(6)}\rangle_n, \hat{H}_2^{(3)}) \simeq 19.95$	$F_Q( D_{0,2}^{(6)}\rangle_n, \hat{H}_2^{(4)}) \simeq 57.12$
$N = 7$	$F_Q( D_{0,2}^{(7)}\rangle_n, \hat{H}_2^{(1)}) \simeq 133.93$	$F_Q( D_{0,2}^{(7)}\rangle_n, \hat{H}_2^{(2)}) \simeq 228.2$	$F_Q( D_{0,2}^{(7)}\rangle_n, \hat{H}_2^{(3)}) \simeq 33.5$	$F_Q( D_{0,2}^{(7)}\rangle_n, \hat{H}_2^{(4)}) \simeq 89.72$
$N = 8$	$F_Q( D_{0,2}^{(8)}\rangle_n, \hat{H}_2^{(1)}) \simeq 226.41$	$F_Q( D_{0,2}^{(8)}\rangle_n, \hat{H}_2^{(2)}) \simeq 359.53$	$F_Q( D_{0,2}^{(8)}\rangle_n, \hat{H}_2^{(3)}) \simeq 56.69$	$F_Q( D_{0,2}^{(8)}\rangle_n, \hat{H}_2^{(4)}) \simeq 144$

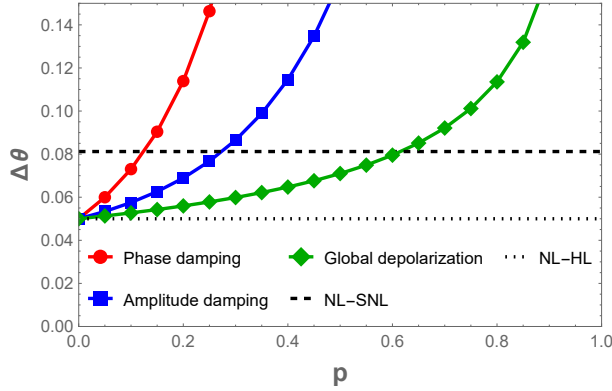


FIG. 4. Comparison of phase sensitivity  $\Delta\theta$  of  $N = 8$ -qubit optimal probe  $|\psi_{(N=8)}^{(2)}\rangle_n = \frac{1}{\sqrt{2}} (|0\rangle_n^{\otimes 8} + |D_{4,5}\rangle_n)$  (see (30)) with parameter encoding generated by the two-body interaction Hamiltonian  $\hat{H}_2^{(2)} = \hat{J}_{\mathbf{n}} + \hat{J}_{\mathbf{n}}^2$ . The plots indicate the relative robustness of the optimal probe under phase damping, amplitude damping, and global depolarization. The NL-SNL and the NL-HL are also indicated.

probes listed in Table IV. These results highlight noise regimes in which the Dicke superposition probes display metrological performance comparable to—and in certain cases outperforming—that of the corresponding optimal states under decoherence. In particular, Fig. 5 shows that both optimal and near-optimal Dicke superpositions respond similarly under global depolarizing noise, exhibiting comparable robustness for either class of probes in this case.

Overall, these results demonstrate that, even in the presence of realistic noise, carefully chosen Dicke superposition probes can retain a substantial metrological advantage over standard benchmarks, while offering a favorable trade-off between phase sensitivity and robustness in nonlinear two-body interaction metrology.

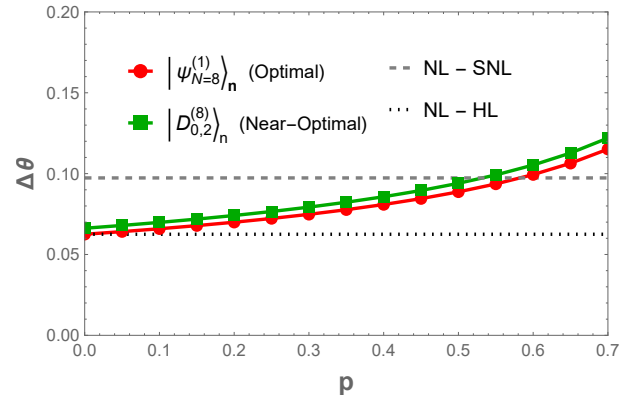


FIG. 5. Comparison of phase sensitivity  $\Delta\theta$  of  $N = 8$ -qubit optimal probe  $|\psi_{(N=8)}^{(2)}\rangle_n = \frac{1}{\sqrt{2}} (|GHZ\rangle_n + |D_{4,4}\rangle_n)$  with that of near optimal Dicke superposition probe  $|D_{0,2}^{(8)}\rangle_n$ , both encoded via the two-body interaction Hamiltonian  $\hat{H}_2^{(1)} = \hat{J}_{\mathbf{n}}^2$ , subjected to global depolarization. The NL-SNL and the NL-HL are displayed for reference.

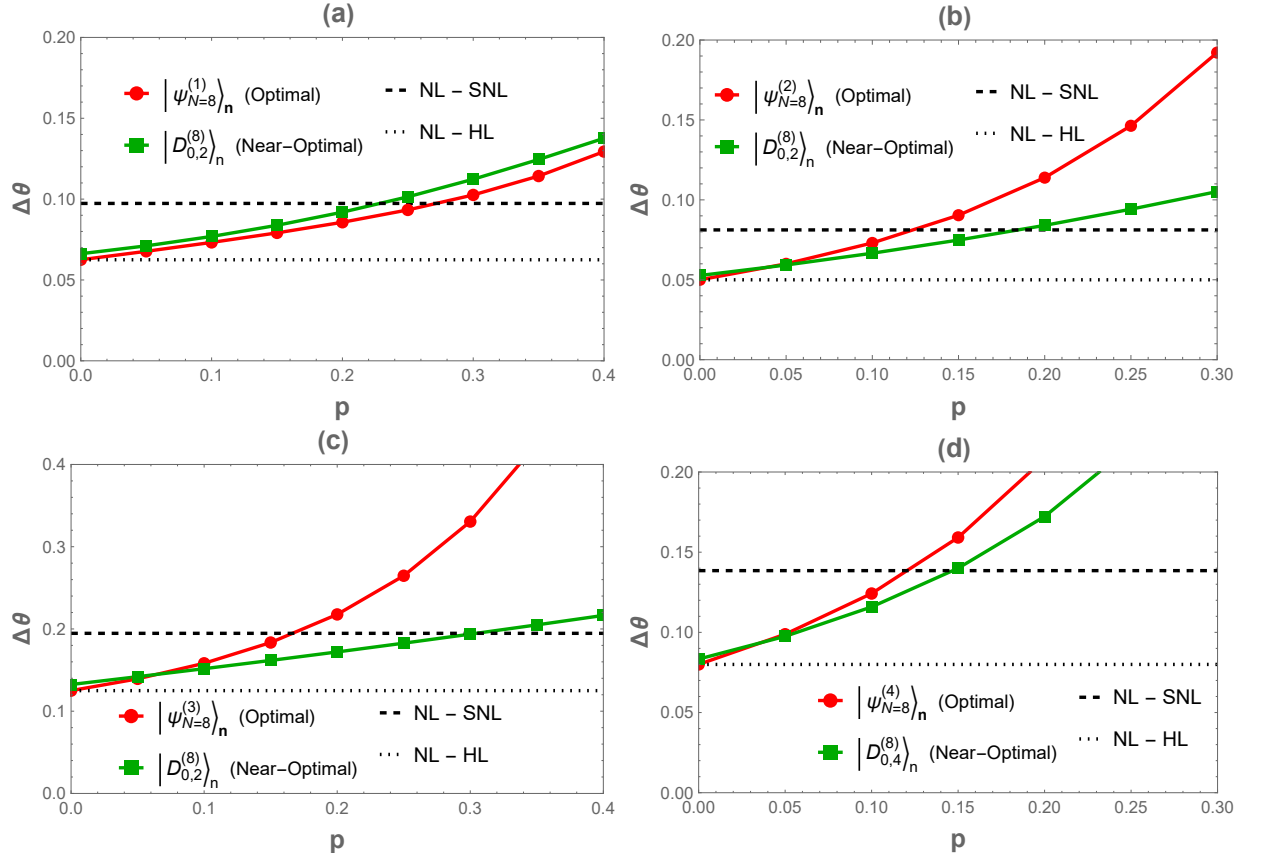


FIG. 6. Comparison of phase sensitivity of optimal probes  $|\psi_{(N=8)}^{(r)}\rangle_n$  with that of near optimal Dicke superposition probes (see Table III) corresponding to the two-body interaction Hamiltonians  $\tilde{H}_2^{(r)}$ ,  $r = 1, 2, 3, 4$ , under phase damping. References in terms of NL-SNL and the NL-HL are indicated.

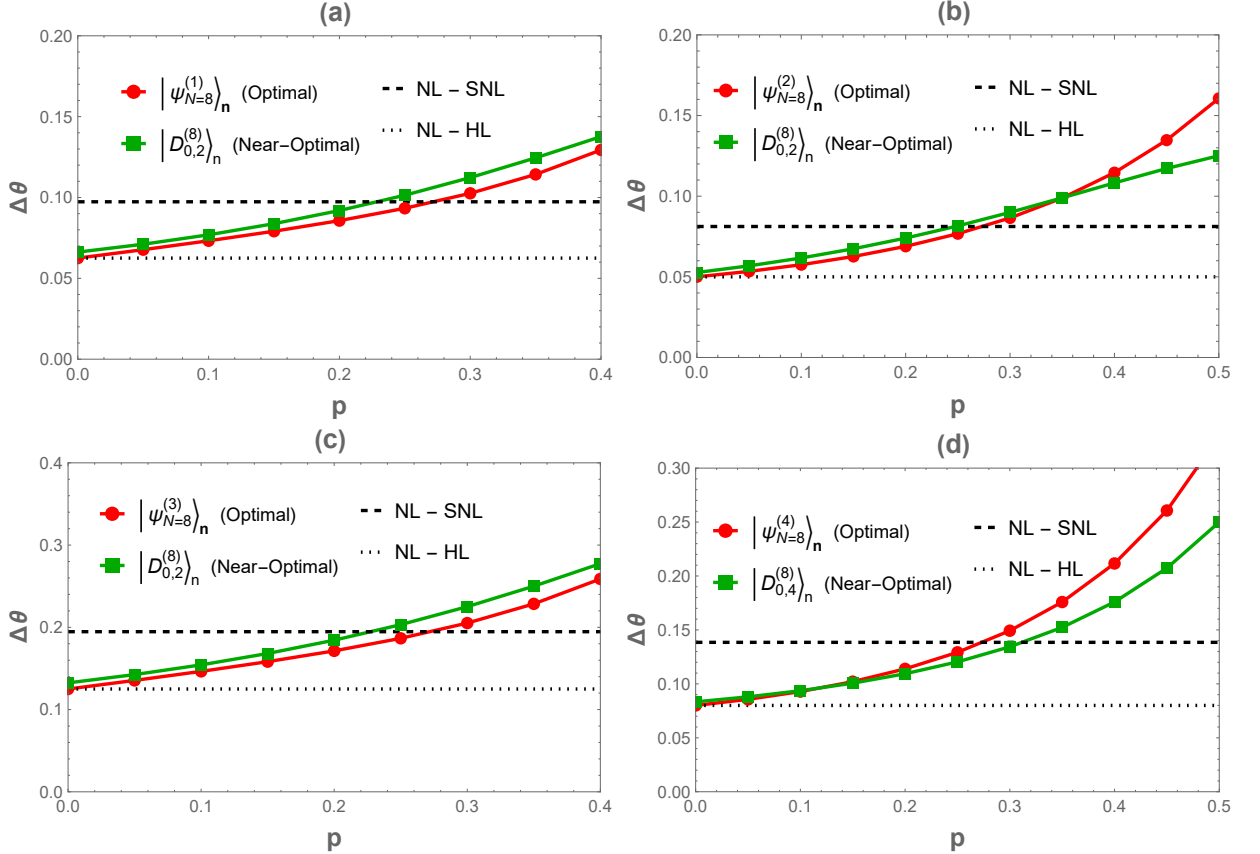


FIG. 7. Comparison of phase sensitivity of  $N = 8$ -qubit optimal probes  $|\psi_{(N=8)}^{(r)}\rangle_n$  with that of near optimal Dicke superposition probes (see Table IV), corresponding to the two-body interaction Hamiltonians  $\hat{H}_2^{(r)}$ ,  $r = 1, 2, 3, 4$ , under phase damping.

## V. CONCLUSIONS

This work has investigated the metrological performance of Dicke superposition probe states in quantum phase estimation protocols governed by linear and nonlinear (two-body) collective spin Hamiltonians, with a particular emphasis on noise resilience under realistic decoherence mechanisms.

Building on the near-optimality of noise-resilient Dicke superposition probes in linear (non-interacting) metrology, a systematic extension to collective two-body interaction generators is carried out. For four representative two-body encoding Hamiltonians  $\hat{H}_2^{(r)}$ ,  $r = 1, 2, 3, 4$ , the maximum and minimum eigenvalues, the corresponding eigenstates, and the resulting QFI are determined analytically, allowing the identification of optimal probe states in the noiseless setting. The associated scaling behavior confirms the emergence of nonlinear metrological limits, with separable probes bounded by a nonlinear SNL scaling and entangled probes capable of attaining the nonlinear HL scaling characteristic of two-body interactions. Near-optimal Dicke superposition probe states were identified by explicitly evaluating and optimizing the Fisher information.

The robustness of both optimal and near-optimal probes has then been examined under local phase damping, local amplitude damping, and global depolarizing noise. While the optimal probes maximize the QFI in the noiseless limit, they are prone to enhanced fragility under certain noise channels, most notably local phase damping. In contrast, the near-optimal Dicke superpo-

sition probes were found to exhibit comparable—and in several cases superior—noise resilience. Under global depolarization, both classes of probes display analogous performance.

Taken together, These results demonstrate that Dicke superposition probes belonging to specific family of states, offer advantage in both linear and nonlinear (two-body interaction) quantum metrology. Even in the presence of realistic noise, these states retain a substantial metrological advantage over classical benchmarks compared to fully optimal probes. This establishes Dicke superposition probes as versatile and noise-resilient resources for Heisenberg and super-Heisenberg limited phase sensing with one- and two-body interaction Hamiltonians.

*Note Added:* During the final stages of preparing this manuscript, we became aware of a recent related work [92] that investigates interaction-enhanced quantum metrology using specific maximal superpositions of symmetric Dicke states. While there is partial conceptual overlap in the use of Dicke superposition states, our work differs substantially in scope and focus. In particular, we identify near-optimal Dicke superposition probes and provide a unified analysis across both linear and two-body metrological schemes, with an explicit emphasis on noise resilience and robustness under realistic decoherence models.

**Acknowledgments:** Sudha and BNK acknowledge the financial support of KITS, K-Tech, Karnataka Govt under the Q-Pragathi project.

---

[1] S. L. Braunstein and C. M. Caves, *Physical Review Letters* **72**, 3439 (1994).

[2] J. J. Bollinger, W. M. Itano, D. J. Wineland, and D. J. Heinzen, *Physical Review A* **54**, R4649 (1996).

[3] S. F. Huelga, C. Macchiavello, T. Pellizzari, A. K. Ekert, M. B. Plenio, and J. I. Cirac, *Physical Review Letters* **79**, 3865 (1997).

[4] V. Giovannetti, S. Lloyd, and L. Maccone, *Science* **306**, 1330 (2004).

[5] D. Leibfried, M. D. Barrett, T. Schaetz, J. Britton, J. Chiaverini, W. M. Itano, J. D. Jost, C. Langer, and D. J. Wineland, *Science* **304**, 1476 (2004).

[6] V. Giovannetti, S. Lloyd, and L. Maccone, *Physical review letters* **96**, 010401 (2006).

[7] M. G. Paris, *International Journal of Quantum Information* **7**, 125 (2009).

[8] L. Pezzè, A. Smerzi, M. K. Oberthaler, R. Schmied, and P. Treutlein, *Reviews of Modern Physics* **90**, 035005 (2018).

[9] P. Hyllus, W. Laskowski, R. Krischek, C. Schwemmer, W. Wieczorek, H. Weinfurter, L. Pezzé, and A. Smerzi, *Physical Review A—Atomic, Molecular, and Optical Physics* **85**, 022321 (2012).

[10] S. Imai, A. Smerzi, and L. Pezzè, *Physical Review A* **111**, L020402 (2025).

[11] A. Bhattacharyya, D. Saha, and U. Sen, *Physical Review A* **112**, L030603 (2025).

[12] B. M. Escher, R. L. de Matos Filho, and L. Davidovich, *Nature Physics* **7**, 406 (2011).

[13] B. J. Falaye, A. G. Adepoju, A. S. Aliyu, M. M. Melchor, M. S. Liman, O. J. Oluwadare, M. D. González-Ramírez, and K. J. Oyewumi, *Scientific Reports* **7**, 16622 (2017).

[14] Z. Zhang and L. Duan, *New Journal of Physics* **16**, 103037 (2014).

[15] Y. Li and Z. Ren, *Physical Review A* **107**, 012403 (2023).

[16] G. Tóth and I. Appelániz, *Journal of Physics A: Mathematical and Theoretical* **47**, 424006 (2014).

[17] I. Appelániz, M. Kleinmann, O. Gühne, and G. Tóth, *Physical Review A* **95**, 032330 (2017).

[18] Z. H. Saleem, M. Perlin, A. Shaji, and S. K. Gray, *Physical Review A* **109**, 052615 (2024).

[19] X. Yin, Z. Xi, X. Lu, Z. Sun, and X. Wang, *Journal of Physics B: Atomic, Molecular and Optical Physics* **44**, 245502 (2011).

[20] Y. Khedif, M. Daoud, and E. H. Sayouty, *Quantum Information Processing* **18**, 45 (2019).

[21] Y. Ouyang, N. Shettell, and D. Markham, *IEEE Transactions on Information Theory* **68**, 1809 (2021).

[22] L. Chen, L. Lu, L. Xia, Y. Lu, S. Zhu, and X. Ma, *Physical Review Letters* **130**, 223601 (2023).

[23] C. W. Helstrom, *Quantum Detection and Estimation Theory* (Academic Press, New York, 1976).

[24] S. M. Kay, *Fundamentals of Statistical Signal Processing, Volume I: Estimation Theory* (Prentice Hall, Englewood Cliffs, NJ, 1993).

[25] D. M. Greenberger, M. A. Horne, A. Shimony, and A. Zeilinger, *American Journal of Physics* **58**, 1131 (1990).

[26] M. Zwierz, C. A. Pérez-Delgado, and P. Kok, *Physical Review A* **85**, 042112 (2012).

[27] A. Luis, *Physics Letters A* **329**, 8 (2004).

[28] S. Boixo, S. T. Flammia, C. M. Caves, and J. M. Geremia, *Physical review letters* **98**, 090401 (2007).

[29] S. Boixo, A. Datta, M. J. Davis, S. T. Flammia, A. Shaji, and C. M. Caves, *Physical review letters* **101**, 040403 (2008).

[30] S. Boixo, A. Datta, S. T. Flammia, A. Shaji, E. Bagan, and C. M. Caves, *Physical Review A—Atomic, Molecular, and Optical Physics* **77**, 012317 (2008).

[31] S. Boixo, A. Datta, M. J. Davis, A. Shaji, A. B. Tacla, and C. M. Caves, *Physical Review A—Atomic, Molecular, and Optical Physics* **80**, 032103 (2009).

[32] L. Pezzé and A. Smerzi, *Physical review letters* **102**, 100401 (2009).

[33] C. Gross, T. Zibold, E. Nicklas, J. Esteve, and M. K. Oberthaler, *Nature* **464**, 1165 (2010).

[34] M. Zwierz, C. A. Pérez-Delgado, and P. Kok, *Physical review letters* **105**, 180402 (2010).

[35] T. Tilma, S. Hamaji, W. J. Munro, and K. Nemoto, *Physical Review A* **81**, 022108 (2010).

[36] D. Braun, G. Adesso, F. Benatti, R. Floreanini, U. Marzolino, M. W. Mitchell, and S. Pirandola, *Reviews of Modern Physics* **90**, 035006 (2018).

[37] K. W. Mahmud, E. Tiesinga, and P. R. Johnson, *Physical Review A* **90**, 041602 (2014).

[38] M. Beau and A. del Campo, *Physical review letters* **119**, 010403 (2017).

[39] M. Napolitano, M. Koschorreck, B. Dubost, N. Behbood, R. Sewell, and M. W. Mitchell, *Nature* **471**, 486 (2011).

[40] D. Tsarev, S. Arakelian, Y.-L. Chuang, R.-K. Lee, and A. Alodjants, *Optics express* **26**, 19583 (2018).

[41] M. Napolitano and M. Mitchell, *New Journal of Physics* **12**, 093016 (2010).

[42] M. M. Rams, P. Sierant, O. Dutta, P. Horodecki, and J. Zakrzewski, *Physical Review X* **8**, 021022 (2018).

[43] X. Deng, S.-L. Chen, M. Zhang, X.-F. Xu, J. Liu, Z. Gao, X.-C. Duan, M.-K. Zhou, L. Cao, and Z.-K. Hu, *Physical Review A* **104**, 012607 (2021).

[44] N. Lordi, J. D. Wilson, M. J. Holland, and J. Combes, *arXiv preprint arXiv:2504.03638* (2025).

[45] J. Yang, S. Pang, A. del Campo, and A. N. Jordan, *Physical Review Research* **4**, 013133 (2022).

[46] Q. Liu, L.-N. Wu, J.-H. Cao, T.-W. Mao, X.-W. Li, S.-F. Guo, M. K. Tey, and L. You, *Nature Physics* **18**, 167 (2022).

[47] Y. Chu, X. Li, and J. Cai, *Physical Review Letters* **130**, 170801 (2023).

[48] F. Ozaydin and A. A. Altintas, *Scientific Reports* **5**, 16360 (2015).

[49] M. J. Woolley, G. J. Milburn, and C. M. Caves, *New Journal of Physics* **10**, 125018 (2008).

[50] R. J. Sewell, M. Napolitano, N. Behbood, G. Colangelo, F. Martin Ciurana, and M. W. Mitchell, *Physical Review X* **4**, 021045 (2014).

[51] X. Nie, J. Huang, Z. Li, W. Zheng, C. Lee, X. Peng, and J. Du, *Science Bulletin* **63**, 469 (2018).

[52] M. W. Mitchell, R. J. Sewell, M. Napolitano, M. Koschorreck, B. Dubost, N. Behbood, and M. Kubasik, *EPJ Web of Conferences* **57**, 03004 (2013).

[53] R. J. Sewell, M. Napolitano, N. Behbood, G. Colangelo, F. Martin Ciurana, and M. W. Mitchell, *Physical Review X* **4**, 021045 (2014).

[54] X. Nie, J. Huang, Z. Li, W. Zheng, C. Lee, X. Peng, and J. Du, *Science Bulletin* **63**, 469 (2018).

[55] R. Liu, Y. Chen, M. Jiang, X. Yang, Z. Wu, Y. Li, H. Yuan, X. Peng, and J. Du, *npj Quantum Information* **7**, 170 (2021).

[56] Y. Kim, S.-Y. Yoo, and Y.-H. Kim, *Physical Review Letters* **128**, 040503 (2022).

[57] R. Demkowicz-Dobrzański, J. Kołodyński, and M. Guć, *Nature communications* **3**, 1063 (2012).

[58] J. Kołodyński and R. Demkowicz-Dobrzański, *New Journal of Physics* **15**, 073043 (2013).

[59] R. Demkowicz-Dobrzański and L. Maccone, *Physical review letters* **113**, 250801 (2014).

[60] S. Alipour, M. Mehboudi, and A. Rezakhani, *Physical review letters* **112**, 120405 (2014).

[61] X.-y. Chen and L.-z. Jiang, *Physical Review A* **101**, 012308 (2020).

[62] E. Majorana, *Il Nuovo Cimento (1924-1942)* **9**, 43 (1932).

[63] R. H. Dicke, *Physical review* **93**, 99 (1954).

[64] F. T. Arecchi, E. Courtens, R. Gilmore, and H. Thomas, *Physical Review A* **6**, 2211 (1972).

[65] M. Kitagawa and M. Ueda, *Physical Review A* **47**, 5138 (1993).

[66] T. Bastin, S. Krins, P. Mathonet, M. Godefroid, L. Lamata, and E. Solano, *Physical review letters* **103**, 070503 (2009).

[67] M. Aulbach, D. Markham, and M. Murao, *New Journal of Physics* **12**, 073025 (2010).

[68] D. J. Markham, *Physical Review A—Atomic, Molecular, and Optical Physics* **83**, 042332 (2011).

[69] A. R. Usha Devi, Sudha, and A. K. Rajagopal, *Quantum Information Processing* **11**, 685 (2012).

[70] B. Lücke, M. Scherer, J. Kruse, L. Pezzé, F. Deuretzbacher, P. Hyllus, O. Topic, J. Peise, W. Ertmer, J. Arlt, L. Santos, A. Smerzi, and C. Klempert, *Science* **334**, 773 (2011).

[71] I. D. Leroux, M. H. Schleier-Smith, and V. Vuletić, *Physical Review Letters* **104**, 073602 (2010).

[72] J. G. Bohnet, B. C. Sawyer, J. W. Britton, M. L. Wall, A. M. Rey, M. Foss-Feig, and J. J. Bollinger, *Science* **352**, 1297 (2016).

[73] J. Zeiher, R. Van Bijnen, P. Schauß, S. Hild, J.-y. Choi, T. Pohl, I. Bloch, and C. Gross, *Nature Physics* **12**, 1095 (2016).

[74] D. Baguette, T. Bastin, and J. Martin, *Physical Review A* **90**, 032314 (2014).

[75] Z. Wang and D. Markham, *Physical review letters* **108**, 210407 (2012).

[76] M. Wiesniak, *Scientific Reports* **11**, 14333 (2021).

[77] C. Marconi, G. Müller-Rigat, J. Romero-Pallejà, J. Tura, and A. Sanpera, *arXiv preprint arXiv:2506.10185* (2025).

[78] W. Dür, G. Vidal, and J. I. Cirac, *Phys. Rev. A* **62**, 062314 (2000).

[79] H. Mikami, Y. Li, and T. Kobayashi, *Physical Review A—Atomic, Molecular, and Optical Physics* **70**, 052308 (2004).

[80] W. Wieczorek, R. Krischek, N. Kiesel, P. Michelberger, G. Tóth, and H. Weinfurter, Phys. Rev. Lett. **103**, 020504 (2009).

[81] W. Wieczorek, N. Kiesel, C. Schmid, and H. Weinfurter, Physical Review A—Atomic, Molecular, and Optical Physics **79**, 022311 (2009).

[82] D. Hume, C.-W. Chou, T. Rosenband, and D. J. Wineland, Physical Review A—Atomic, Molecular, and Optical Physics **80**, 052302 (2009).

[83] P. Zarkeshian, C. Deshmukh, N. Sinclair, S. Goyal, G. Aguilar, P. Lefebvre, M. G. Puigibert, V. Verma, F. Marsili, M. Shaw, *et al.*, Nature communications **8**, 906 (2017).

[84] Y.-Q. Zou, L.-N. Wu, Q. Liu, X.-Y. Luo, S.-F. Guo, J.-H. Cao, M. K. Tey, and L. You, Proceedings of the National Academy of Sciences **115**, 6381 (2018).

[85] Y. Wang and B. M. Terhal, Physical Review A **104**, 032407 (2021).

[86] J. Martin, O. Giraud, P. A. Braun, D. Braun, and T. Bastin, Physical Review A **81**, 062347 (2010).

[87] M. A. Nielsen and I. L. Chuang, *Quantum computation and quantum information* (Cambridge university press, 2010).

[88] D. Leibfried, R. Blatt, C. Monroe, and D. Wineland, Rev. Mod. Phys. **75**, 281 (2003).

[89] M. Saffman, T. G. Walker, and K. Mølmer, Rev. Mod. Phys. **82**, 2313 (2010).

[90] H. Ritsch, P. Domokos, F. Brennecke, and T. Esslinger, Rev. Mod. Phys. **85**, 553 (2013).

[91] P. Ribeiro, J. Vidal, and R. Mosseri, Phys. Rev. Lett. **99**, 050402 (2007).

[92] Y. Li and Z. Ren, Physica A: Statistical Mechanics and its Applications **682**, 131192 (2026).